15th CIRP Conference on Modelling of Machining Operations

Evaluating Residual Stresses Induced by Drilling of Ti-6Al-4V Alloy by Using an Experimental-Numerical Methodology

J.P. Nobre[a,b,*] and J.C. Outeiro[b,c]

[a]*School of Mechanical, Industrial and Aeronautical Engineering, University of the Witwatersrand, Johannesburg, WITS 2050, South Africa*
[b]*CEMDRX, Physics Department, University of Coimbra, Coimbra, 3000, Portugal*
[c]*Arts et Metiers ParisTech, LaBoMaP, Rue Porte de Paris, 71250 Cluny, France*

* Corresponding author. Tel.: +27-011-70177301; fax: ++27-011-70177302. *E-mail address:* joao.nobre@wits.ac.za

Abstract

An experimental-numerical methodology is applied to evaluate the residual stresses induced by drilling of Ti-6Al-4V alloy. The influence of ultra-high cutting speeds on the residual stress distribution is analysed. These ultra-high cutting speeds are produced by a turbine system powered by compressed air, which are commonly used in the hole-drilling equipment for residual stress measurements. The applied hybrid methodology has demonstrated an important role on the optimization of the drilling operations parameters for an improved residual stress distribution.

Peer-review under responsibility of the International Scientific Committee of the "15th Conference on Modelling of Machining Operations
Keywords: Residual stress; Drilling; Titanium; Finite element method (FEM)

1. Introduction

Residual stresses may have either beneficial or detrimental effects (part distortion, premature cracking, decreasing or increasing the final mean stress during cyclic loading, etc.), with the correspondent effect on the service life of the final parts [1]. Therefore, the determination of residual stresses induced by manufacturing processes assumes high practical importance, either for optimization of final manufacturing processes, either for validation of specific simulation software used [2], always aiming to improve the functional performance and service life of structural parts.

Nomenclature

A	Reduction of area at fracture
E	Modulus of Elasticity (Young's modulus)
ν	Poisson's ratio
$R_{p0.2}$	Yield stress
R_m	Tensile strength
$\Delta\varepsilon$	Induced drilling strain relaxation
$\Delta\varepsilon_{exp}$	Experimentally determined drilling strain relaxation
F_1	Minimum applied load during tensile tests
F_2	Maximum applied load during tensile tests
ΔF	Differential load (F_2-F_1)
σ_{RS}	Residual stress
σ_{1cal}	Calibration stress corresponding to F_1
σ_{2cal}	Calibration stress corresponding to F_2
σ_1	Resulting stress when F_1 is applied (σ_{RS}+σ_{1cal})
σ_2	Resulting stress when F_2 is applied (σ_{RS}+σ_{2cal})
$\Delta\sigma$	Calibration stress (σ_2+σ_1)
Z	Hole depth
APDL	ANSYS Parametric Design Language
FEM	Finite element method
IHD	Incremental hole-drilling
UHSD	Ultra high speed drilling

The drilling operation is one of the most common machining operations. However, only few works have been performed regarding the residual stresses induced by thermo-mechanical effects during this important machining operation. Bolted joints, for example, are widely used in mechanical construction [3] and the control of the structural integrity of

the hole-drilled parts is very important, for which the residual stresses induced by drilling is a main parameter to take into account. On the other hand, the so-called hole-drilling technique and, in particular, the incremental hole-drilling technique (IHD) is a well-accepted mechanical technique for residual stress measurement [4]. The principle of the IHD technique was the base for the proposed methodology. This technique consists on drilling a small hole in the surface of the test material (1-3 mm diameter) and to measure the strain relaxation induced by the hole on the residual stress field that is intended to be determined [4]. The influence of the drilling operation itself on the existent residual stress state is crucial for a reliable application of this technique. This technique was very well developed for isotropic materials, especially, for steels, for which an ultra-high speed drilling (UHSD) procedure was proposed by Flaman [5]. However, its application to other materials, in particular to difficult-to-machining materials, needs a better knowledge of the induced drilling stresses. In fact, almost all publications related with residual stresses induced by drilling have been performed to improve the reliability of IHD [6-10]. Although the high importance of the knowledge of the induced drilling stresses, regarding the drilling optimization, almost no studies exist on this issue. This is due to the high difficulty and complexity for determining induced drilling stresses. Bore walls are not easily accessible for the different residual stress measurement techniques available. In general, almost all studies regarding the determination of induced drilling stresses during IHD [7-9] were based on measuring the strain relaxation in metallic specimens previously subjected to thermal treatments for residual stress relaxation. However, it is well known that thermal treatments are not one hundred percent effective. On the other hand, this procedure cannot be applied to polymer matrix composites. Considering these restrictions, and to study the applicability of IHD to glass fibre reinforced polymers, in particular, and to polymer matrix composites in general, Nobre et al. [11] proposed a new methodology to determine the induced drilling strains, based on the principles of the IHD technique. In this work, this methodology was applied to study the induced drilling stresses in a titanium Ti-6Al-4V alloy subjected to UHSD, using special carbide coated end mills. The cutting speed of UHSD was analysed by modifying the air pressure of the air turbine system used. Especially emphasis was put on developing a numerical model of the drilling operation. The main objective, however, is the demonstration of the importance of the proposed methodology for optimizing drilling operations. Their parameters can be improved by controlling the final induced drilling residual stresses. The study of the computer numerical control of drilling operation using twist drills, to perform cylindrical holes in the same alloy, is currently under study and will be presented in the near future.

2. Experimental-Numerical Methodology

The residual strains and stresses, induced during the drilling operation, due to the thermo-mechanical effects of the cutting process, can be used to evaluate the quality of the drilling operation. The methodology used in this work permits the induced drilling stresses to be determined. The quantification is based on an experimental calibration procedure, where the specimens are incrementally drilled under a tensile calibration stress, followed by a numerical simulation of the experimental test. The comparison of the experimental and predicted data allows the residual strains to be evaluated. Therefore, the proposed methodology should be performed in two different phases, an experimental and a numerical simulation phase. The great advantage of this methodology is the independency from the materials under test and drilling operation applied. It means that the presented methodology can be applied to any drilling operation and test material, without any restriction. It is only necessary to consider the constitutive laws of the test material during the numerical simulation phase.

The first shortcoming to be solved during the experimental phase, since the proposed methodology needs no special previous treatment of the material, is how to take into account the initial residual stresses, i.e., the residual stresses existing in the material before drilling. If, in the case of metallic materials, stress relief by thermal treatment can be applied, without a complete guaranty of its complete removal, in the case of polymer matrix composites this procedure cannot even be applied. Therefore, a method to eliminate this effect was developed based on the principle of superposition. This principle can be understood by analysing Fig. 1.

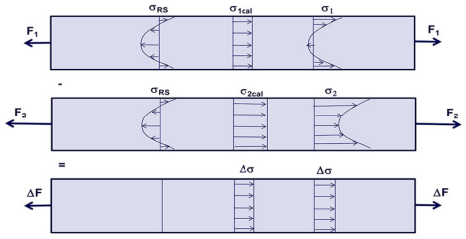

Fig. 1. Elimination of the initial residual stresses by using the superposition principle.

Thus, the calibration stress to be considered during the experiments will be equal to the differential stress $\Delta\sigma$, based on the differential load ΔF (see Fig. 1), instead the use of an absolute stress, σ_{1cal} or σ_{2cal}, due to a given level of applied load to the specimen, F_1 or F_2, respectively. The magnitude of the greatest load, F_2, must be chosen considering that the material only behaves in the elastic regime and also taken into account the stress concentration effect due to the hole presence. This way, the effect of the initial residual stress, σ_{RS}, will be separated from the calibration stress ($\Delta\sigma$) and the strain relaxation measured during the drilling tests will only be due to the calibration stress $\Delta\sigma$ applied. In practice, a modified tensile test machine was used to apply the tensile stresses to the specimens. The loads are controlled by a precision load cell and the strains by electric strain gauges.

In the experimental phase, the stress-strain behaviour of the material is studied firstly, by loading and unloading the specimens, until the maximum applied load, F_2. The initial strains, for the minimum and maximum applied loads, F_1 and F_2, respectively, are recorded for the determination of the strain relaxation after drilling each depth increment.

Secondly, the specimen is loaded to the lowest load F_1 and the first depth increment is drilled. After measuring and recording the strains arising around the hole, using special strain gauge rosettes, the specimen is loaded to the greatest load F_2 and the strains measured and recorded again. The specimen is then unloaded to F_1 and the second depth increment is drilled. These steps are repeated until a depth, at least, equal to the radius of the hole, is attained. Fig. 2 illustrates the experimental procedure.

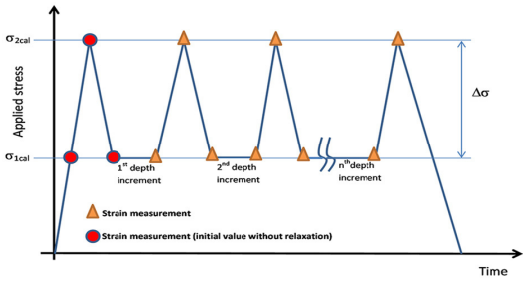

Fig. 2. Graphical representation of the experimental procedure.

Based on the initial strain values, the strain relaxation after each depth increment can be determined. This way, a set of curves of strain relaxation versus hole depth, corresponding to the calibration stress imposed ($\Delta\sigma$), is obtained. These curves, which take into account all thermo-mechanical effects of the cutting process, are further compared with ideal numerical ones determined by finite element simulation.

In the subsequent numerical simulation phase, the experimental calibration procedure described above is simulated using the finite element method (FEM). This numerical simulation approach is carried out considering all parameters used during the experimental phase, i.e., hole diameter, hole depth, size and number of depth increments, strain gauge area related with the strain gauge rosette used and elastic properties of the material. This way, ideal in-depth strain relaxation curves, corresponding to a given applied calibration stress, ($\Delta\sigma$), can be determined. FEM analysis only considers the geometrical effect of the hole presence on the imposed uniaxial stress field and is carried out assuming linear elastic material behaviour. The obtained strain relaxation vs. depth curves can be considered ideal ones, i.e., where the thermo-mechanical effects due to the drilling operation is not taken into account. This is an ideal drilling operation where the material is removed without any contact effect, i.e., without friction and plastic deformation that happen during real cutting processes. Thus, the differences observed between the experimentally and numerically obtained strain relaxation, in each incremental depth drilled, are essentially due to the residual strains induced by the thermo-mechanical effects of cutting. For optimization purposes it might be preferable to determine a percentage error, related to the strains induced by the drilling operation. Assuming that experimentally determined strain relaxation as a function of depth is $\Delta\varepsilon_{exp}(z)$ and the numerically determined strain relaxation (ideal case) is $\Delta\varepsilon_{num}(z)$, the induced drilling strains $\Delta\varepsilon(z)$ should be calculated by:

$$\Delta\varepsilon(z) = \Delta\varepsilon_{num}(z) - \Delta\varepsilon_{exp}(z) \quad (1)$$

Since the applied calibration stress is tensile, both strain relaxation values, $\Delta\varepsilon_{num}(z)$ and $\Delta\varepsilon_{exp}(z)$, will be negative. According to equation (1), the induced drilling strains can lead to tensile or compressive stresses, depending on the magnitude of $\Delta\varepsilon_{num}(z)$ and $\Delta\varepsilon_{exp}(z)$. Thus, if:

$$|\Delta\varepsilon_{num}(z)| > |\Delta\varepsilon_{exp}(z)| \Rightarrow \Delta\varepsilon(z) < 0 \Rightarrow \text{Tensile stresses} \quad (2)$$

$$|\Delta\varepsilon_{num}(z)| < |\Delta\varepsilon_{exp}(z)| \Rightarrow \Delta\varepsilon(z) > 0 \Rightarrow \text{Compress. stresses} \quad (3)$$

However, it should be noted that the magnitude of the final stresses will be always related with the gradient of the strain relaxation-depth curves. A percentage error, $\Lambda(z)$, as a function of depth, can be also determined by:

$$\Lambda(z) = \frac{|\Delta\varepsilon(z)|}{\varepsilon_{num}(z)} \times 100 \ [\%] \quad (4)$$

3. Material, experimental and numerical procedures

Titanium alloy of the series Ti-6Al-4V, widely used in aeronautical structures, was selected for this study. Table 1 shows its main mechanical properties. Fig. 3 shows the specimens geometry used in the experimental phase. The width in the measurement region of the specimens was selected according to the standard dimensions of the three element strain-gauge rosette used (ASTM type B standard rosette [4]).

Table 1. Mechanical properties of Ti-6Al-4V alloy.

$R_{p0.2}$ [MPa]	R_m [MPa]	E [GPa]	ν	A [%]
880	950	114	0.34	14

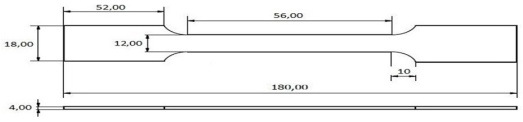

Fig. 3. Geometry of the specimens used in the tensile tests.

For the experimental tests, a horizontal tensile test machine, shown in Fig. 4, was used. The machine was equipped with a purpose-designed grip system, an accurate load cell, a three-point support for mounting the IHD equipment and an anti-bending system, composed by a brass screw, nut and lock-nut, as also shown in Fig. 4.

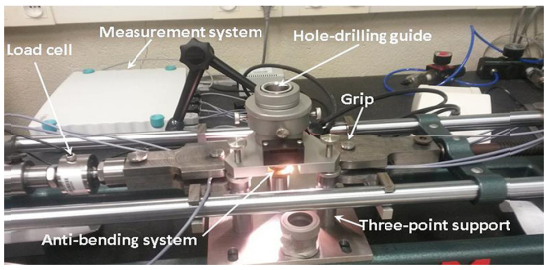

Fig. 4. Tensile test machine used during the experimental phase.

The specimens were clamped and subjected to two different load levels, for a given differential calibration stress ($\Delta\sigma$), as already explained before. Table 2 shows the mean parameters used during the tensile calibration tests. The effective maximum stress (~563 MPa) around the hole is lower than the material yield stress (880 MPa).

Table 2. Tensile test parameters.

Cross Section	Minimum load		Maximum Load			
Area mm^2	F_1 KN	σ_{1cal} MPa	F_2 KN	σ_{2cal} MPa	$\Delta\sigma$ MPa	$R_{p0.2}$ MPa
48	1	21	10	209	187.5	880

IHD equipment (RS-200 system from Vishay®) was used for the drilling operation. This system uses a turbine system powered on by compressed air, which enables ultra-high rotation speeds. As shown in table 3, in the present study the rotation speed has been varied by changing the air pressure between 2.5 bar and 3.5 bar. Below 2.5 bar no enough torque was developed to cut the material. Above 3.5 bar was not possible to keep the end mill well clamped. The rotation speed was evaluated using frequency analysis of the sound produced by the turbine through a FFT (Fast Fourier Transformation) algorithm. As shown in Fig. 5, for the range of air pressure used, the rotation speed varied between 100000 rpm and 125000 rpm. For a given rotation speed, the hole-drilling test was repeated several times for statistical analysis. For all tests the feed rate was very low and performed intermittently (i.e., touch/remove the end mill when drilling each depth increment), to minimise the thermal effects induced by friction. The drilling operation was always performed for the minimum applied load at the centre of the ASTM type B rosette. Coated tungsten carbide end mills with 1.6 mm diameter and six teeth were used in all tests (a new end mill per test). The holes were made incrementally using 50-100µm as minimum depth increment. After each depth increment, the values of the strain relaxation, arising around the hole, were recorded for the two load levels, F_1 and F_2. The experiments were repeated until a total hole depth approximately equal to the hole radius (≈ 0.9 mm).

Table 3. Hole-drilling parameters.

Air pressure [bar]	Cutting Speed [m/min]	Number of tests	Feed rate [mm/min]	Hole diameter [mm]
2.5	534	2	< 0.01	1.83
2.8	550	2	< 0.01	1.79
3	565	5	< 0.01	1.83
3.5	581	1	< 0.01	1.82

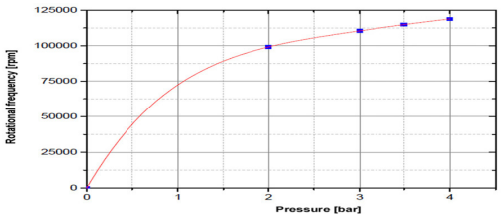

Fig. 5. End-mills rotational speed as a function of the air pressure for turbine feeding.

ANSYS Parametric Design Language (APDL) [11] was used to develop the numerical simulation model. Quadratic 8 node 3D structural solid elements (SOLID185 [11]) was selected. The FEM model has been parameterized to be applied to different situations, to minimize the need of changing of the APDL scripts. The finite element mesh was developed considering ¼ of the model (two symmetric planes). During the numerical simulation phase, hole-drilling was always simulated, incrementally, at the centre of the FEM model, using "birth and death" ANSYS code features [11]. The depth increments were equal to those used during the experiments (~50 µm). Fig. 56 shows the mesh used in the FEM model. The paths on the model correspond to the grids of each strain-gauge of the standard ASTM type B rosette used in this study. During the post-processing phase, the nodal strain values are automatically integrated over the surface area corresponding to each strain-gauge.

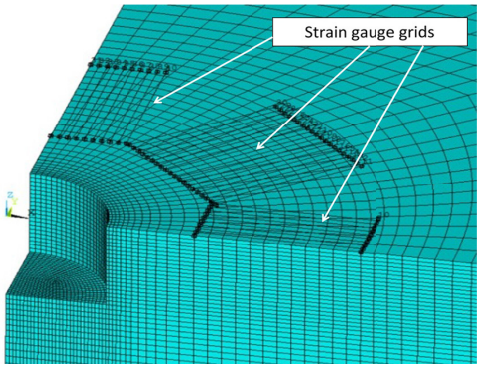

Fig. 6. Finite element mesh near 1 mm hole depth and 1.83 mm hole diameter (SG grids for ASTM type A rosette).

4. Results and Discussion

Fig. 7 shows the stress-strain behaviour of the Ti-6Al-4V alloy, determined experimentally, in the range of the applied loads used during the experimental tests. The Young's modulus and Poisson's ratio are in good agreement with the values presented in the literature for the Ti-6Al-4V alloy – see also table 1.

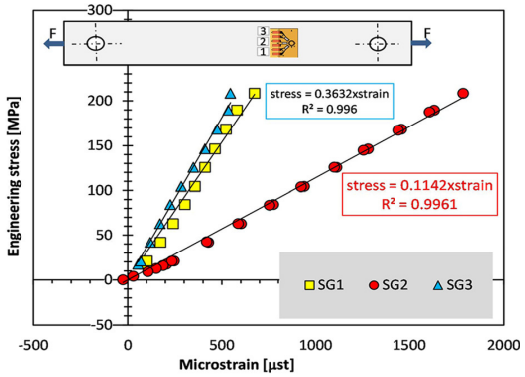

Fig. 7. Stress-strain behaviour of the Ti-6Al-4V alloy.

In respect of the hole-drilling tests, performed on the specimens subjected to tensile stresses, whose parameters are

shown in table 2, a set of strain-depth relaxation curves were determined, for each cutting speed. Fig. 8 shows, as example, the results obtained experimentally (measured) for a cutting speed 550 m/min. These results are expected, considering the level and the sign of the calibration stress applied (+187.5 MPa) (see table 2 and Fig. 2). Applied tensile stresses imply negative strain relaxation values [4].

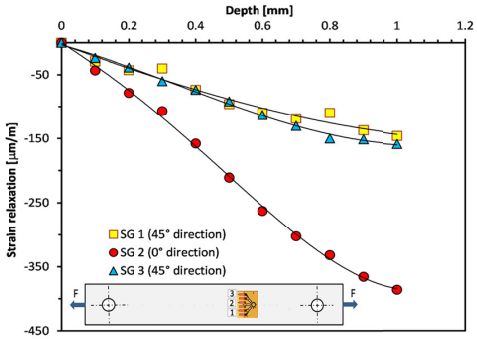

Fig. 8. Measured in-depth strain relaxation distribution (stress of +187.5 MPa, d = 1.83 mm, cutting speed 550 m/min).

A numerical simulation was performed using the same geometrical parameters and the same differential calibration stress of 187.5 MPa, applied during the experimental tests. Fig. 9 shows the predicted (FEM) stress distribution around a hole with different depths, for the above-mentioned stress applied in X direction. An interesting conclusion is that the stress concentration effect increases with the increase of the hole depth.

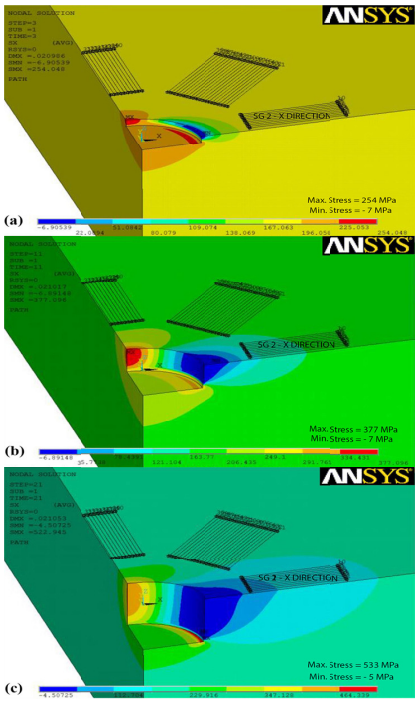

Fig. 9. Predicted stress distribution (σ_x) around a hole (1.83 mm; 187.5 MPa). Depth: 0.1 mm (a), 0.5 mm (b) and 1.0 mm (c).

Fig. 10 shows the in-depth predicted strain relaxation distributions in the longitudinal direction (0°, direction of the axis of the specimens and applied load (SG2)), cross direction (90°) and at 45° (SG1 and SG3). The next step consists into compare measured (experimental) and predicted (FEM) in-depth strain relaxation distributions.

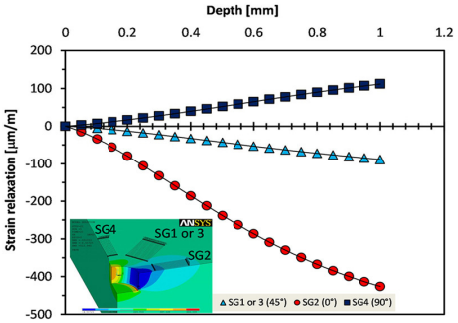

Fig. 10. Predicted in-depth strain relaxation distribution (stress of 187.5 MPa in X direction (SG2); 1.83 mm hole diameter).

Figs. 11 show this comparison for the longitudinal direction and for different cutting speeds used in the experimental tests. The experimental curves are the average curves that better fits all tests performed for each cutting speed (see table 3) and the error bars reflect the standard deviation. Higher standard deviations were found for the two highest cutting speeds.

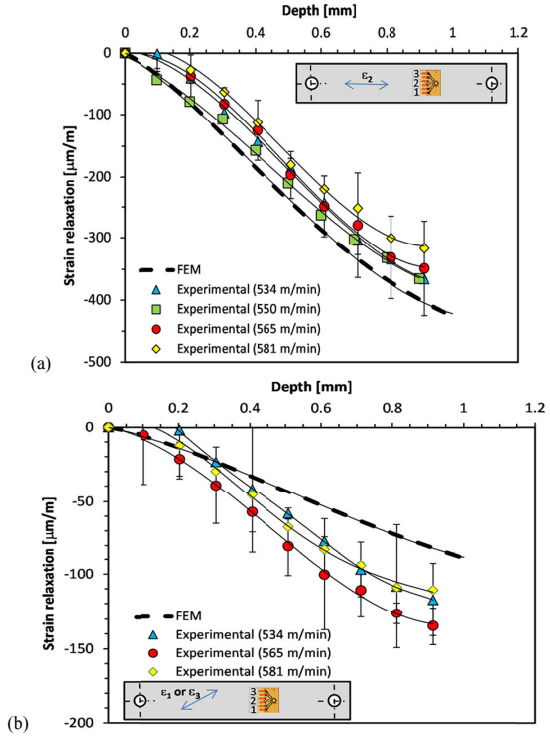

Fig. 11. Experimental vs. FEM in-depth strain relaxation distributions. a) 0° direction and b) 45° direction.

As shown in Fig. 11 (a), the variation in the cutting speed was not sufficient to produce significant changes in the in-depth strain relaxation distributions. However, the difference between predicted and measured results slightly increases with the increase of cutting speed, although the large error bars observed for the two highest cutting speeds. This figure also shows that for the same depth, all measured strain relaxations are lower than the predicted one.

Since negative strains imply the appearance of tensile residual stresses (see equations (1) and (2)), experimentally the applied stress will be less tensile than the predicted one. In all cases, the average values corresponding to all experimental tests are inside the standard deviation found for the cutting speed of 565 m/min. It can be concluded that the obtained results clearly show a good repeatability. If the experimental values are lower than the predicted ones for longitudinal direction, the inverse is true for 45° direction – see Fig. 11 b).

Considering equation (1), the strain relaxation *vs*. depth curves, corresponding to the induced drilling strains, can be determined. For sake of clarity, Fig. 12 shows these curves for two cutting speeds: 534 m/min and 565 m/min. As expected the induced drilling strains were similar for both cases.

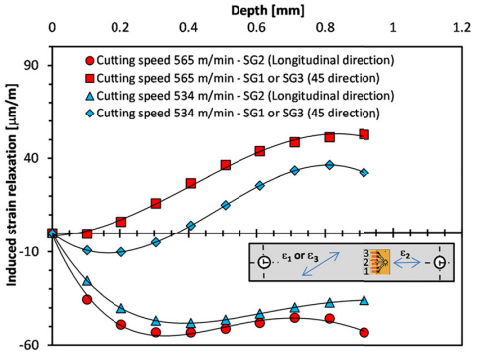

Fig. 12. Induced strain relaxation vs. depth curves for two different hole-drilling conditions.

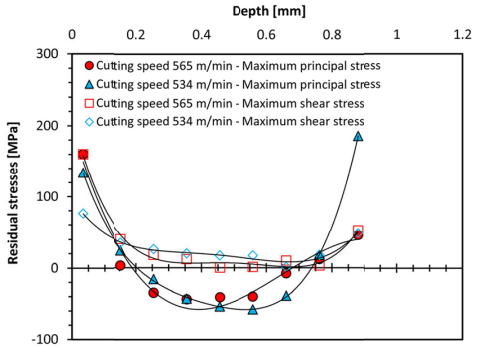

Fig. 13. Induced drilling stresses for two drilling conditions.

The corresponding induced drilling residual stresses are similar for both cases, as shown in Fig. 13. These stresses were determined using the so-called integral method for residual stress determination by IHD [4,12]. Near the surface the stress state is more adverse for the case of higher the cutting speed, i.e., 565 m/min, where higher shear stress state arises. The U shape of the in-depth distribution of the induced drilling stresses must be noted. UHSD induced relatively high tensile residual stresses near the surface, which become slightly compressive in the intermediate layers, where the shear stress is almost negligible. In deepest layers, the residual stresses become tensile again. Regarding the application of IHD for measuring residual stresses in the titanium alloy studied, some care must be taken when analysing the values near the surface and for deepest layers.

5. Conclusions

- Induced drilling stresses due to UHSD of Ti-6Al-4V alloy were determined using an experimental-numerical methodology.
- No substantial differences were found due to the variation of the ultra-high cutting speeds used in the tests. For all cases, in depth principal maximum stress profiles present a U shape with tensile stresses near the surface and in the deeper layers, higher than the compressive stresses found in the intermediate depth layers.
- The results present a good repeatability and, therefore, the proposed methodology seems to be an important tool for the optimization of the drilling operation parameters, regarding improving the induced drilling stresses.
- IHD can be applied for measuring residual stresses in Ti-6Al-4V alloys. However, some care should be considered for the values determined in the near surface layers and in the deepest layers.

Acknowledgements

J.P. Nobre gratefully acknowledges the financial support received from the Department of Science and Technology (DST) of the South African Government, through the program Horizon 2020 Seed Funding under the ESASTAP Plus Programme, which made this work possible.

References

[1] Scholtes B. Eigenspannungen in Mechanisch Randschichtverformten Werkstoffzuständen: Ursachen, Ermittlung und Bewertung. Oberursel: DGM, Informationsgesellschaft mbH; 1991.

[2] Jawahir IS, Brinksmeier E, M'Saoubi R, Aspinwall DK, Outeiro JC, Meyer D, Umbrello D, Jayal AD. Surface integrity in material removal processes. CIRP Annals 2011; 60/2:603-626.

[3] Handbook of bolts and bolted joints. In: Bickford J, Nassar S, editors. New York: CRC press; 1998.

[4] ASTM E837-13a. Standard test method for determining residual stresses by the hole-drilling strain-gage method. ASTM International; 2013.

[5] Flaman MT. Brief investigation of induced drilling stresses in the center-hole method of residual-stress measurement. Exp. Mech. 1982; 22:26-30.

[6] Rendler NJ, Vigness I. Hole-drilling strain-gage method of measuring residual stresses. Exp. Mech. 1966; 6:577-586.

[7] Flaman MT, Herring JA. Comparison of four hole-producing techniques for the center-hole residual-stress measurement method. Exp. Tech. 1985; 9:30-32.

[8] Weng CC, Lin YC, Chou CP, A new approach for determining the induced drilling stressesin the hole-drilling method of residual-stress measurement. Exp. Tech. 1992; 16:33-35.

[9] Honner M, Litos P, Svantner M. Thermography analyses of the hole-drilling residual stress measuring technique. Infra. Phys. & Tech. 2004; 45:131-142.

[10] Nobre JP, Stiffel J-H, Nau A, Outeiro JC, Batista AC, Paepegem W, Scholtes B. Induced drilling strains in glass fibre reinforced epoxy composites. CIRP Annals 2013; 60(2):87-90.

[11] ANSYS. Mechanical APDL Release 15.0. Houston: SAS Inc.; 2013.

[12] Nobre JP, Dias AM, Domingos AJ, Morais R, Reis, MJ. A windows-based software package to evaluate residual stresses by the incremental hole-drilling technique. Comp. Appl. Eng. Educ. 2009; 17(3):351–362.